Dispersion of Single-Walled Carbon Nanotubes Using Nucleobase-Containing Poly(acrylamide) Polymers

Darryl Fong,[a] Zan Hua,[b] Thomas R. Wilks,[b] Rachel K. O'Reilly,*[b] and Alex Adronov*[a]

[a]*Department of Chemistry, McMaster University, Hamilton, ON, Canada*

[b]*Department of Chemistry, University of Warwick, Coventry, United Kingdom*

[*] Prof. Alex Adronov
Department of Chemistry
McMaster University
1280 Main St. W.
Hamilton, ON
L8S 4M1
Email: adronov@mcmaster.ca
Tel: (905) 525-9140 x23514
Fax: (905) 521-2773

[*] Prof. Rachel O'Reilly
Department of Chemistry
University of Warwick
Coventry, United Kingdom
Email: R.K.O-Reilly@warwick.ac.uk
Tel: +44 (0) 247 652 3236
Fax: +44 (0) 247 652 4112

Abstract

Single-walled carbon nanotubes (SWNTs) possess extraordinary properties, but suffer from poor solubility and a lack of purity. Of the possible routes available to solubilize and purify nanotube samples, the use of noncovalent functionalization is ideal as carbon nanotube properties are not deleteriously affected. A multitude of different dispersants have been investigated thus far, but of particular interest is deoxyribonucleic acid (DNA), which has previously been demonstrated to effectively separate metallic and semiconducting carbon nanotubes. Here, we investigate the ability of synthetic nucleobase-containing poly(acrylamide) polymers to produce stable nanotube dispersions in organic solvents. Polymers bearing different nucleobase and backbone structures, as well as block copolymers with different block sequences were investigated. Polymer:SWNT mass ratios and solvent compositions were optimized for the nucleobase-functionalized polymers, and semiconducting and metallic SWNT populations were identified by a combination of UV-Vis-NIR absorption, Raman, and fluorescence spectroscopy. These results demonstrate the capacity for synthetic DNA analogues to disperse SWNTs in organic media.

Keywords: Nucleobase Polymers; Carbon Nanotubes; Supramolecular Functionalization; Nanotube Dispersion.

Introduction

Since the discovery of single-walled carbon nanotubes (SWNTs) in 1991,[1] much effort has been devoted to utilizing their extraordinary structural,[2] mechanical,[3] and optoelectronic[4–6] properties. This is non-trivial, however, since as-produced SWNTs are an impure mixture of amorphous carbon, leftover metal catalyst particles, and both semiconducting and metallic SWNTs.[7] Due to inter-tube π–π interactions, SWNTs form bundles that are insoluble in typical aqueous and organic solvents.[8] In order

to take advantage of the exceptional properties possessed by SWNTs, nanotube exfoliation and solubilization are imperative, typically relying on either covalent or noncovalent functionalization methods.[9–11] Covalent functionalization disrupts the extended π-system of the SWNT sidewall, destroying many of the advantageous SWNT properties.[11] Meanwhile, noncovalent functionalization maintains the integrity of the SWNT sidewall, which has led to significant interest in this area of research.[12–14] For noncovalent functionalization, a dispersant is required to prevent SWNT bundle re-aggregation and render SWNTs soluble. Numerous dispersants have been identified, including surfactants,[15–17] aromatic compounds,[18–20] conjugated polymers,[21–25] proteins,[26–28] polysaccharide-iodine complexes,[29] and deoxyribonucleic acids (DNA).[30–32] Of the aforementioned dispersant types, single-stranded DNA is unique in its ability to selectively disperse individual semiconducting (sc-SWNT) chiralities using specific oligonucleotide sequences, usually after a secondary purification step such as ion exchange chromatography.[33] Although impressive, a drawback hindering large-scale DNA-based SWNT purification is the prohibitive cost of the dispersant. A dispersant that combines the selectivity of DNA with cost-effective, scalable production would therefore be highly attractive. Recently, nucleobase functionalities have been incorporated within synthetic polymers in an effort to achieve templated polymerizations and supramolecular self-assembly.[34–38] Polymerization of monomers that have been functionalized with one of the natural nucleobases (adenine, thymine, guanine, or cytosine) produces polymers with nucleobase-containing side chains. Although less architecturally controlled and sequence specific than DNA, these synthetic analogues have been shown to undergo self-assembly processes controlled by Watson-Crick base pairing and can be prepared on a relatively large scale.[39] Here, we examine the interactions of a new class of nucleobase-functionalized poly(acrylamide) (PAAm) polymers with SWNTs, and their ability to form stable nanotube dispersions through π-stacking of the nucleobases with the SWNT sidewall.

Results and Discussion

To probe the supramolecular interactions of nucleobase-containing PAAm polymers with SWNTs, we prepared a series of homopolymers containing appended adenine (**P1**), cytosine (**P2**), or thymine (**P3**) nucleobases, according to literature procedures (Fig. 1 and supporting information, Figs. S1-S3).[39] Each of the polymerizations were carried out for 2 h at 70 °C in a mixture of water and 1,4-dioxane prior to analysis by ^{1}H NMR spectroscopy and size exclusion chromatography (SEC). It should be noted that the guanine containing monomer (GAm) exhibited poor solubility in common aqueous and organic solvents, and no well-defined polymer could be formed under a wide range of polymerization conditions. Therefore, we focused on the polymers containing adenine, cytosine, and thymine (**P1**-**P3**). These polymers were sparingly soluble in water (~0.1 mg mL^{-1} for **P1** and **P3**; < 0.5 mg mL^{-1} for **P2**) and moderately soluble in DMF (> 20 mg mL^{-1} for **P3**, > 2 mg mL^{-1} for **P1**, and < 0.5 mg mL^{-1} for **P2**). SEC analysis showed that **P1** had a number-average molecular weight (M_n) of 8.1 kDa with a dispersity ($Đ_M$) of 1.04 while **P3** had an M_n of 8.2 kDa with a $Đ_M$ of 1.03 (Figs. S4-S5). Due to the low solubility of **P2** in DMF, SEC analysis was not possible for this polymer sample. However, ^{1}H NMR end group analysis of **P2** indicated ~19 repeat units, which suggested an M_n of ~4.5 kDa (Fig. S6).

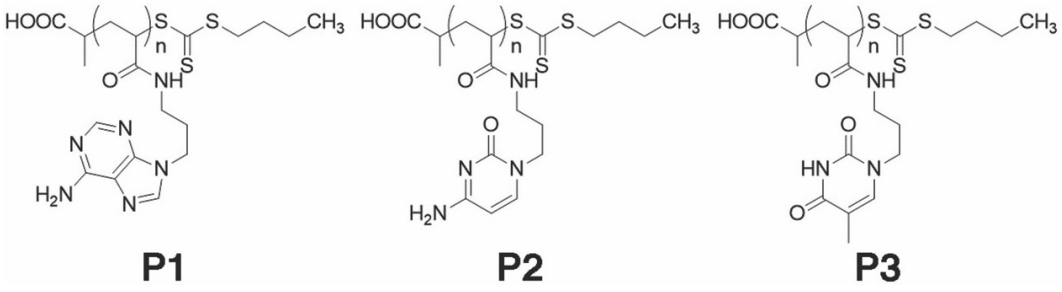

Figure 1. Chemical structures of nucleobase-containing homopolymers used in this study. **P1** contained adenine (A), **P2** cytosine (C), and **P3** thymine (T).

Supramolecular polymer-SWNT complexes of **P1**-**P3** were prepared with raw HiPCO SWNTs following modifications of previously reported procedures.[40] To begin optimizing the dispersion parameters, **P3** was chosen due to its excellent solubility in DMF. A generic dispersion protocol was as follows: 3 mg of polymer was dissolved in organic solvent, HiPCO SWNTs were added, and the mixture sonicated for 2 h in a bath sonicator chilled with ice. The sample was then centrifuged at 8 346 *g* for 30 minutes, followed by careful removal of the supernatant and characterization as isolated. Unfortunately, using 3 mg of **P3** in 4 mL of THF or DMF (polymer concentration of 0.75 mg mL^{-1}) and sonicating with 2 mg of raw HiPCO SWNTs (1.5:1 polymer:SWNT mass ratio) did not result in stable SWNT dispersions. Although **P3** was sparingly soluble in THF, it was highly soluble in DMF, yet surprisingly, no stable dispersions were obtained in either of these solvents. We hypothesized that, despite the polymer's solubility in DMF, its higher viscosity resulted in difficulty exfoliating SWNT bundles via sonication. To alleviate the high viscosity, yet retain solubility, a mixture of DMF and THF (50/50 vol/vol) was attempted and found to produce stable dispersions. This solvent mixture was then utilized as a starting point for the subsequent studies.

To determine the minimum amount of **P3** required to produce stable SWNT dispersions, a polymer:SWNT mass ratio study was performed. The mass ratio was varied from 2.5:1 to 10:1 in 8 mL of 50/50 THF:DMF (polymer concentration of 0.38 mg mL^{-1}) and SWNT dispersions were characterized by absorption spectroscopy (Fig. 2a). Nanotube absorption features arise from the interband transitions of the van Hove singularities, resulting in specific nanotube chiralities having characteristic transition energies. These transition energies depend on respective SWNT diameters and chiralities, and the absorption features in the observed range can be grouped into three categories: two semi-conducting regions, S_{11} (830-1600 nm) and S_{22} (600-800 nm), and a metallic region, M_{11} (440-645 nm).[41] The spectra for SWNT dispersions prepared using all three **P3**:SWNT ratios showed sharp peaks in the S_{11} and S_{22}

regions, suggesting that **P3** efficiently exfoliated sc-SWNTs in 50/50 THF:DMF. The presence of a broad, featureless absorption background in the spectrum between 400 and 800 nm also indicated the presence of metallic SWNTs (m-SWNTs), which was corroborated by the dark brown-black colour of the **P3**-SWNT dispersions, indicating a lack of nanotube selectivity (Fig. 3). Although these SWNT dispersions were spectroscopically similar, the dispersions prepared using 2.5:1 and 5:1 **P3**:SWNT mass ratios were unstable overnight, while the SWNT dispersion prepared using a 10:1 **P3**:SWNT mass ratio was stable for at least several weeks. Thus, a mass ratio of 10:1 polymer:SWNT was used in further studies.

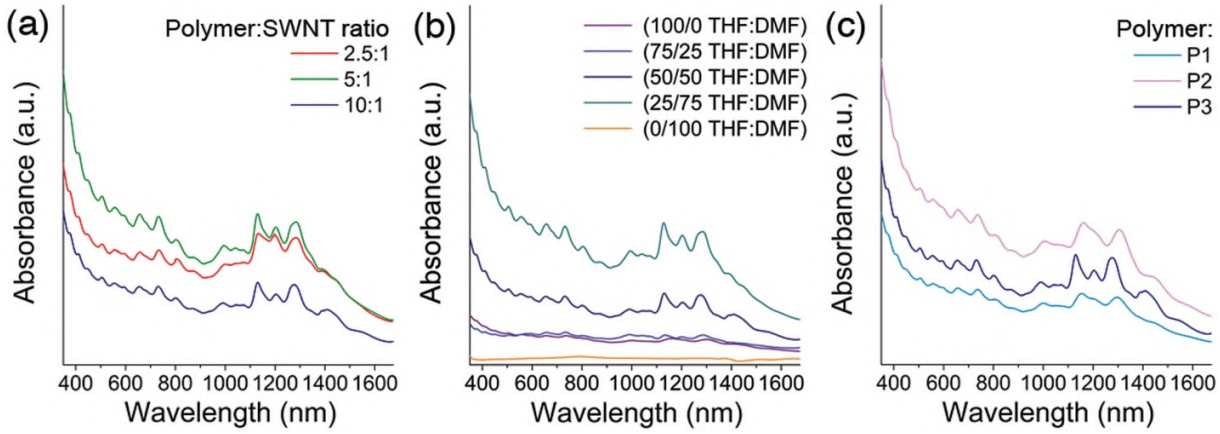

Figure 2. UV-Vis-NIR spectra of polymer:SWNT complexes: (a) **P3** dispersions prepared using 2.5:1 to 10:1 **P3**:SWNT mass ratios in 50/50 THF:DMF, (b) **P3** dispersions prepared in solvent mixtures of THF and DMF with a 10:1 **P3**:SWNT mass ratio, and (c) dispersions prepared with **P1**-**P3** using a 10:1 polymer:SWNT mass ratio in 50/50 THF:DMF.

Figure 3. Photograph of **P3**-SWNT prepared with a polymer:nanotube mass ratio of (left to right) 2.5:1, 5:1, or 10:1 in a 50/50 mixture of THF:DMF.

Dispersion preparation conditions were further optimized by varying the ratio of the two co-solvents. Using **P3** as the dispersant at a mass ratio of 10:1 **P3**:SWNT, the ratio of THF to DMF was varied from neat THF to neat DMF in 25% increments, and the nanotube dispersion was characterized by absorption spectroscopy (Fig. 2b). When > 75% THF was used, featureless absorption spectra without an intense absorption background were obtained, suggesting that a dilute dispersion of SWNT bundles was present. This showed the inability of **P3** to effectively exfoliate HiPCO SWNTs when too much of a poor solvent (THF) was present. These SWNT dispersions were also metastable, flocculating within an hour after centrifugation. On the other extreme, neat DMF resulted in no SWNT dispersion, even when polymer concentration was diluted, which typically improves colloidal stability.[42] We believe that this lends credence to the hypothesis that the inability to obtain SWNT dispersions in neat DMF was a consequence of solvent viscosity hindering sonication energy from temporarily exfoliating SWNT bundles and enabling interactions with polymers. The optimal DMF content that allowed for the dispersion of HiPCO SWNTs using **P3** was found to be 50-75%. The spectra for these SWNT dispersions showed sharp peaks in the S_{11} and S_{22} regions, suggesting that **P3** efficiently exfoliated sc-SWNTs in these solvent mixtures. Again, the broad, featureless absorption background and the brown-black colour of these dispersions signified the presence of m-SWNTs (Fig. S17). These results highlighted the importance of striking a balance between polymer solubility and solvent viscosity. If the polymer is sparingly soluble in a solvent mixture, it is unlikely that a stable SWNT dispersion will result. Likewise, if the solvent is too viscous, sonication cannot temporarily breakup SWNT bundles to allow for the polymer to coat the SWNT surface.

With these results in hand, we performed a dispersion study using **P1**-**P3** with the optimized conditions (10:1 polymer:SWNT mass ratio and 50/50 THF:DMF) and characterized the resulting dispersions using absorption spectroscopy (Fig. 2c and Fig S15). For the dispersions produced using **P1** and **P2**, broad peaks were apparent in the S_{11} and S_{22} regions of the absorption spectra. This suggested

that some degree of SWNT bundling was present in these samples. In contrast, the **P3**-SWNT dispersion had sharp peaks in the S_{11} and S_{22} regions, suggesting excellent exfoliation of HiPCO SWNTs when using **P3** (the thymine containing polymer). It is interesting to note that, based on absorption spectroscopy, the most soluble polymer appeared to produce the most exfoliated SWNT dispersion. We hypothesize that the colloidal stability observed is correlated to polymer solubility as favourable solvent-polymer interactions hinder undesired polymer–polymer interactions that could result in SWNT flocculation.

To further investigate the SWNT dispersions produced by **P1**-**P3**, resonance Raman spectroscopy was performed. This technique allows for the examination of both m- and sc-SWNT species within a given sample,[43] and utilizes laser excitation wavelengths that overlap with the van Hove singularities present in the 1D density of states for a particular SWNT.[44] As the electronic transitions depend on nanotube chirality and diameter, only a subset of the total nanotube population will be observed for each individual excitation wavelength.[45]

A total of four dispersions were investigated using resonance Raman spectroscopy: the **P1**-SWNT and **P2**-SWNT dispersions prepared using optimized conditions, and two of the **P3**-SWNT dispersions (the dispersion prepared using optimized conditions and the dispersion prepared in 25/75 THF:DMF). Thin film samples were prepared from the polymer-SWNT dispersions by drop-casting onto silicon wafers heated at 50 °C in an oven; heating was necessary to quickly evaporate DMF. A reference SWNT sample was also prepared by sonicating a small amount of the SWNT starting material in $CHCl_3$ and making a solid film with the same drop-casting method, in this case without sample heating. Raman spectra were collected using three excitation wavelengths: 514, 633, and 785 nm. These excitation wavelengths have previously been shown to be adequate for characterizing the electronic character of HiPCO SWNT samples, as both m- and sc-SWNTs can be separately probed.[46] Fig. 4 shows the radial breathing mode (RBM) regions from the four samples at each excitation wavelength (full Raman spectra

are provided in the supporting information, Fig. S16). All Raman spectra were normalized to the G-band at ~1590 cm^{-1} and offset for clarity.

While mainly sc-SWNTs are in resonance with the 785 nm excitation wavelength for HiPCO SWNTs, a few larger diameter metallic species, most notably the (16,7) and (12,9) chiralities, have been observed in the low-frequency region.[47,48] In our case, none of the polymer-SWNT samples exhibited any signals below 200 cm^{-1}, which indicated the absence of large diameter m-SWNTs in all samples. The most intense peak in the raw SWNT spectrum occurred at 265 cm^{-1} and corresponded to (10,2) SWNTs, which are in resonance with this excitation wavelength when bundled.[49] This peak is often referred to as the "bundling peak" and can be used to identify bundling in a nanotube sample, but only if (10,2) SWNTs are present. Fig. 4a shows that a decrease in the bundling peak occurred when SWNTs were dispersed with **P3** (for quantitation of peak areas, see Table S2), giving further evidence that SWNTs were efficiently exfoliated using this polymer. When comparing the **P3**-SWNT dispersions prepared in 50/50 THF:DMF versus 25/75 THF:DMF, the bundling peak for the sample prepared in 50/50 THF:DMF was more suppressed (Table S2), suggesting that SWNT exfoliation happened to a greater extent in 50/50 THF:DMF. In contrast, the bundling peaks for **P1**-SWNT and **P2**-SWNT dispersions were more intense, with the **P2**-SWNT dispersion having the most intense bundling peak. This suggests that, under identical preparation conditions, SWNT exfoliation was poor when using **P1** and negligible when using **P2**. The ability of these polymers to exfoliate HiPCO SWNTs followed the trend of DMF solubility (**P3** > **P1** > **P2**, thymine > adenine > cytosine) and confirmed the trend observed with absorption spectroscopy. Based on these observations, it appears that polymer solubility is imperative in order to produce stable polymer-SWNT dispersions.

To obtain a complete picture of the nanotube populations dispersed using the polymer series, Raman spectra excited at 633 nm and 514 nm were also examined. Upon excitation at 633 nm, both m- and sc-SWNTs are in resonance (Fig. 4b). For HiPCO SWNTs, m-SWNT features are found at ~175-

230 cm^{-1}, while sc-SWNTs give rise to peaks at ~230-300 cm^{-1}.[41,46] Both m- and sc-SWNT features were observed in all polymer-SWNT samples. Upon excitation at 514 nm, dominant RBM features are typically between 225 and 290 cm^{-1}, arising from m-SWNTs.[48] For all polymers, these peaks were observed (Fig. 4c), suggesting that these nucleobase-containing polymers dispersed small diameter m-SWNTs in addition to sc-SWNTs. This observation was corroborated by analysis of the G-band region at this excitation wavelength, which is shown in the supporting information, Fig. S16. The G-band consists of two peaks: a lower frequency G^- and a higher frequency G^+. For sc-SWNTs, both the G^- and G^+ have Lorentzian line shapes, but for m-SWNTs the G^- exhibits a broad shoulder at low wavenumbers (1500-1580 cm^{-1}), referred to as the Breit–Wigner–Fano (BWF) line shape.[50] A broad G^- was observed for all SWNT samples, confirming that m-SWNTs were present.

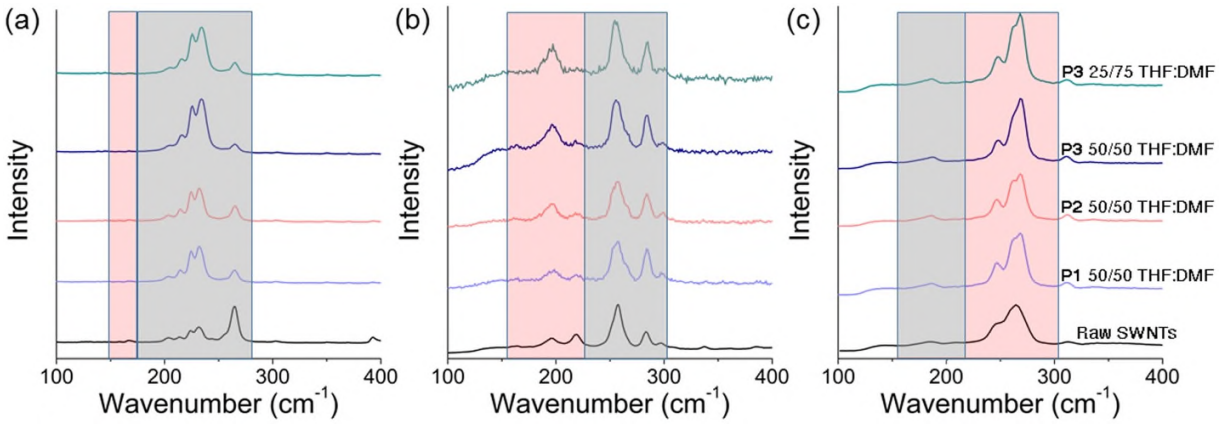

Figure 4. RBM regions of the Raman spectra using (a) 785 nm, (b) 633 nm, and (c) 514 nm excitation wavelengths. The gray boxes denote the locations of signals arising from sc-SWNTs, while the pink boxes represent the locations of signals arising from m-SWNTs.

Photoluminescence (PL) maps were recorded for both **P3**-SWNT samples, as they contained well-exfoliated SWNTs (Fig. 5). The locations of various SWNT fluorescence maxima were assigned according to previously published data.[51] PL signals were observed for the **P3**-SWNT dispersion

prepared in 50/50 THF:DMF, with the most intense peak corresponding to the (9,4) chirality (Fig. 5a). Although the concentration of the **P3**-SWNT sample prepared in 25/75 THF:DMF was matched by obtaining comparable absorption intensities for the (9,4) chirality at 1101 nm (see supporting information, Fig. S17), PL signals for this sample were not observed when plotted on the same scale. The observed fluorescence quenching could be attributed to two possibilities: the presence of nanotube bundles or the enrichment of exfoliated m-SWNTs. The Raman data suggested that the **P3**-SWNT sample prepared in 25/75 THF:DMF contained more bundles (based on the more intense bundling peak), and so the increased presence of SWNT bundles was a plausible explanation for the observed contrast. It is less likely that the difference in fluorescence intensity was due to differences in m-SWNT concentration, as the metallic features present for both dispersions appeared almost identical by absorption and Raman spectroscopy.

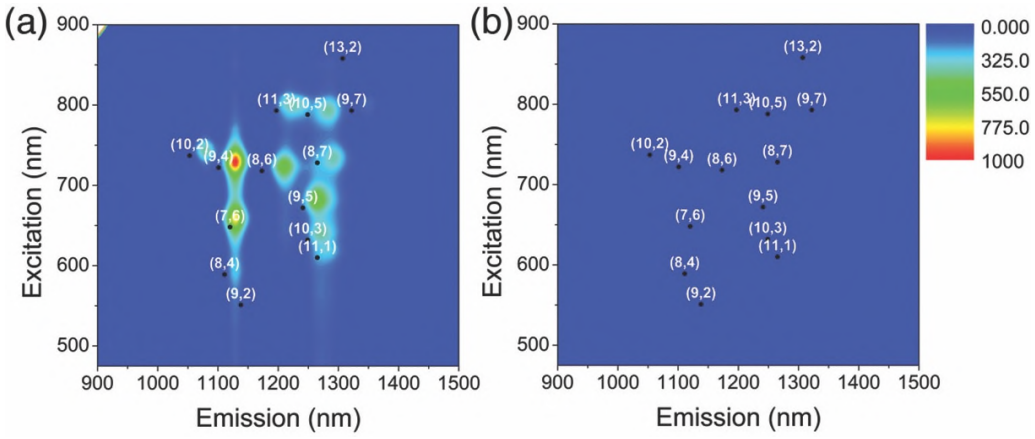

Figure 5. PL maps corresponding to **P3**-SWNT prepared in (a) 50/50 THF:DMF or (b) 25/75 THF:DMF at a similar concentration and plotted on the same scale. The locations of SWNT fluorescence maxima were assigned according to previously published data.[51]

With these results in hand, we examined the effect of polymer molecular weight on thymine-containing PAAm homopolymers. Previously, we demonstrated that the molecular weight of conjugated polymers can influence the SWNT dispersion selectivity, so we investigated whether this factor is important in the present case.[52] We prepared three additional molecular weights of the thymine-

containing PAAm homopolymers using the aforementioned polymerization methods, obtaining a series of polymers with DPs of 10, 40, and 60 (**P4**-**P6**) (See supporting information, Fig. S7-S8 and Table S1). Polymer-SWNT dispersions were prepared as per the optimized protocol (vide supra) and characterized by absorption and Raman spectroscopy. The absorption spectra for **P5**-SWNT and **P6**-SWNT had sharp peaks in the S_{11} and S_{22} regions, which indicated that exfoliated sc-SWNTs were dispersed (Fig. 6a). Both spectra also had a large exponential background absorption, indicating the presence of m-SWNTs. Compared to **P3**-SWNT, these two polymer-SWNT samples had spectral features that were very similar, which suggested that the SWNT populations they dispersed were nearly identical. Raman spectroscopy validated this interpretation (See supporting information, Fig. S18). Meanwhile, the absorption spectrum for **P4**-SWNT was ill-defined and not intense. The Raman spectrum of the **P4**-SWNT sample exhibited a relatively intense bundling peak at ~265 cm^{-1} when excited at 785 nm, indicating that the sample contained nanotube bundles. These data suggested that a minimum number of repeat units (~20) was required for this polymer class to produce well-exfoliated SWNT dispersions. Above this threshold, the dispersed SWNT populations appeared to remain consistent, which is unsurprising as the π–π interactions between the polymer and SWNT sidewall remains similar within this polymer series.

In a parallel study, we varied the polymer backbone structure while maintaining an identical DP (~20) and nucleobase functionality (thymine) to investigate its effect on dispersed SWNT populations. This involved investigation of polymers with polystyrene- (PVBT, **P7**) and poly(methylmethacrylate)-like (PTMA, **P8**) backbones (Figure 7 and supporting information, Figs. S9-S10). Polymer-SWNT dispersions were prepared using the optimized protocol (vide supra) and characterized by absorption and Raman spectroscopy. The absorption spectra for **P7** and **P8** indicated the presence of both m-SWNTs and sc-SWNTs, as per the analysis mentioned above (Fig. 6b provides comparison to **P3** data). The SWNT populations dispersed by these polymers appeared to be similar regardless of the backbone architecture, as corroborated by Raman spectroscopy (Fig. S19). This suggested that SWNT interactions

were unaffected by the polymer backbone composition, and were primarily influenced by the π–π interactions between the nucleobase and SWNT.

In addition to the aforementioned polymers, we prepared a series of block copolymers containing *N*-acryloylmorpholine (NAM) and thymine-containing PTAm (1:1 overall block ratio) to investigate the effect of block copolymer architecture on SWNT dispersions. The relative amounts of NAM and TAm were held constant, while producing a diblock (**P9**), triblock (**P10**), and octablock (**P11**) copolymer (Fig. 7 and supporting information, Figs. S11-S13 and Table S3)**.** Polymer-SWNT dispersions were prepared using the optimized protocol (vide supra) and characterized by absorption and Raman spectroscopy. As per prior analyses, the dispersed SWNT populations appeared to be unchanged regardless of the block copolymer configuration. These data are consistent with the hypothesis that the primary influence on successful SWNT dispersion and selectivity was the polymer-SWNT π–π interaction, rather than the nature of the colloidal dispersion stabilizer. Again, the data demonstrated the inherent flexibility of this polymer class, as the dispersed SWNT populations were unaffected by backbone architecture.

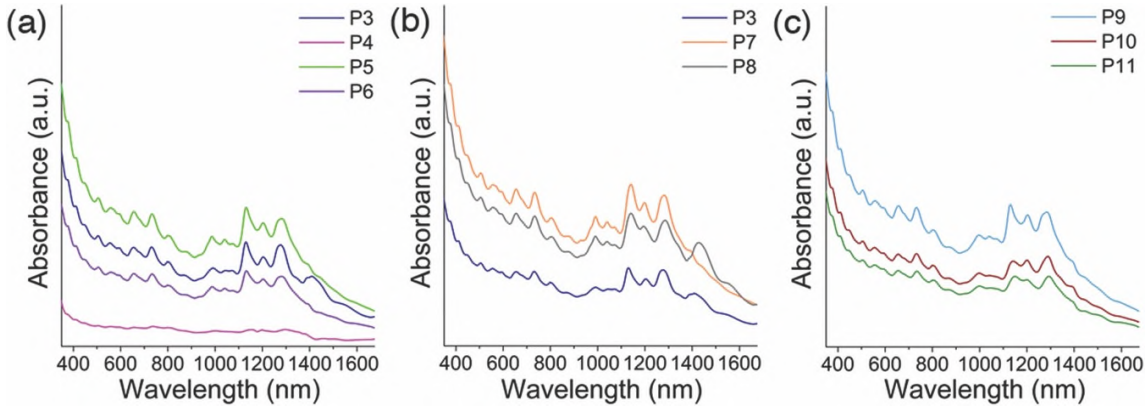

Figure 6. UV-Vis-NIR spectra of polymer:SWNT complexes: (a) molecular weight study of thymine-containing PAAm homopolymers, with a DP of 10-60 (**P3-P6**), (b) backbone architecture study with poly(acrylamide) (**P3**), polystyrene (**P7**), and poly(methylmethacrylate) (**P8**) backbones, and (c) diblock (**P9**), triblock (**P10**), and octablock (**P11**) NAM-TAm block copolymers.

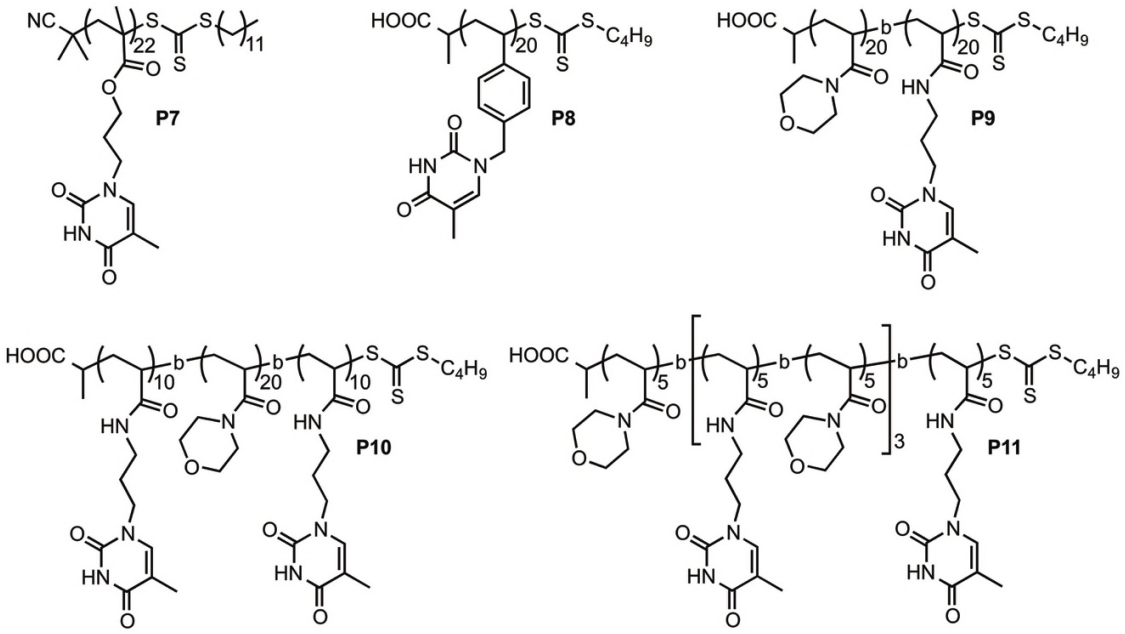

Figure 7. Structures of polymers with different backbone structure, **P7** and **P8**, as well as different block architecture, **P9**-**P11**.

Conclusions

We have demonstrated that nucleobase-containing polymers are capable of forming stable dispersions with SWNTs. Our results highlight the importance of identifying the balance between polymer solubility and solvent mixture viscosity when preparing SWNT dispersions. When the solvent mixture was controlled, the most soluble polymer, **P3**, a thymine functionalized acrylamide, formed the most stable, well-exfoliated SWNT dispersions. Although interactions with SWNTs were not selective, it is interesting that different nucleobases within the polymers led to different degrees of dispersion. This polymer class demonstrates flexibility with respect to backbone chemistry, and allows for many potential synthetic avenues to be pursued. These results warrant the continued investigation of these polymers to begin identifying structure-selectivity relationships in SWNT dispersions.

Supporting Information. Full experimental details, spectral and chromatographic data, and sample images.

Acknowledgements

Financial support from the Natural Science and Engineering Research Council (NSERC) of Canada and the European Research Council (grant no: 615142) is gratefully acknowledged. D.F. is grateful for support through an NSERC CGS-D scholarship and Z.H. thanks the China Scholarship Council for financial support. The Materials GRP at Warwick is also acknowledged for financial support.

References

1. Iijima, S. *Nature*, 1991, **354**, 56–58.
2. Terrones, M. *Annu. Rev. Mater. Res.*, 2003, **33**, 419–501.
3. Saito, R., Dresselhaus, G., Dresselahus, M. Physical Properties of Carbon Nanotubes, 1998.
4. O'Connell, M. J., Bachilo, S. M., Huffman, C. B., Moore, V. C., Strano, M. S., Haroz, E. H., Rialon, K. L., Boul, P. J., Noon, W. H., Kittrell, C., Ma, J., Hauge, R. H., Weisman, R. B., Smalley, R. E. *Science*, 2002, **297**, 593–596.
5. Bachilo, S. M., Strano, M. S., Kittrell, C., Hauge, R. H., Smalley, R. E., Weisman, R. B. *Science*, 2002, **298**, 2361–2366.
6. Kataura, H., Kumazawa, Y., Maniwa, Y., Umezu, I., Suzuki, S., Ohtsuka, Y., Achiba, Y. *Synth. Met.*, 1999, **103**, 2555–2558.
7. Baughman, R. H., Zakhidov, A. A., de Heer, W. A. *Science*, 2002, **297**, 787–792.
8. Tasis, D., Tagmatarchis, N., Bianco, A., Prato, M. *Chem. Rev.*, 2006, **106**, 1105–1136.
9. Hirsch, A. *Angew. Chem. Int. Ed.*, 2002, **41**, 1853–1859.
10. Britz, D. A., Khlobystov, A. N. *Chem. Soc. Rev.*, 2006, **35**, 637–659.

11. Campidelli, S., Klumpp, C., Bianco, A., Guldi, D. M., Prato, M. *J. Phys. Org. Chem.*, 2006, **19**, 531–539.

12. Zhao, Y. L., Stoddart, J. F. *Acc. Chem. Res.*, 2009, **42**, 1161–1171.

13. Bilalis, P., Katsigiannopoulos, D., Avgeropoulos, A., Sakellariou, G. *RSC Adv.*, 2014, **4**, 2911–2934.

14. Gavrel, G., Jousselme, B., Filoramo, A., Campidelli, S. *Top. Curr. Chem.*, 2014, **348**, 95–126.

15. Islam, M. F., Rojas, E., Bergey, D. M., Johnson, A. T., Yodh, A. G. *Nano Lett.*, 2003, **3**, 269–273.

16. Moore, V. C., Strano, M. S., Haroz, E. H., Hauge, R. H., Smalley, R. E., Schmidt, J., Talmon, Y. *Nano Lett.*, 2003, **3**, 1379–1382.

17. Gong, X., Liu, J., Baskaran, S., Voise, R. D., Young, J. S. *Chem. Mater.*, 2000, **12**, 1049–1052.

18. Yang, K., Zhu, L., Xing, B. *Environ. Sci. Technol.*, 2006, **40**, 1855–1861.

19. Tomonari, Y., Murakami, H., Nakashima, N. *Chem. Eur. J.*, 2006, **12**, 4027–4034.

20. Chen, R. J., Zhang, Y., Wang, D., Dai, H. *J. Am. Chem. Soc.*, 2001, **123**, 3838–3839.

21. Chen, J., Liu, H., Weimer, W. A., Halls, M. D., Waldeck, D. H., Walker, G. C. *J. Am. Chem. Soc.*, 2002, **124**, 9034–9035.

22. Star, A., Stoddart, J. F., Steuerman, D., Diehl, M., Boukai, A., Wong, E. W., Yang, X., Chung, S. W., Choi, H., Heath, J. R. *Angew. Chem. Int. Ed.*, 2001, **40**, 1721–1725.

23. Nish, A., Hwang, J.-Y., Doig, J., Nicholas, R. J. *Nat. Nanotechnol.*, 2007, **2**, 640–646.

24. Yim, C. Bin, Dijkgraaf, I., Merkx, R., Versluis, C., Eek, A., Mulder, G. E., Rijkers, D. T. S., Boerman, O. C., Liskamp, R. M. J. *J. Med. Chem.*, 2010, **53**, 3944–3953.

25. Cheng, F. Y., Imin, P., Lazar, S., Botton, G. A., de Silveira, G., Marinov, O., Deen, J., Adronov, A. *Macromolecules*, 2008, **41**, 9869–9874.

26. Guo, Z., Sadler, P. J., Tsang, S. C. *Adv. Mater.*, 1998, **10**, 701–703.

27. Balavoine, F., Schultz, P., Richard, C., Mallouh, V. V., Ebbesen, T. W., Mioskowski, C. *Angew.*

Chem. Int. Ed., 1999, **38**, 1912–1915.

28. Bradley, K., Briman, M., Star, A., Gruner, G. *Nano Lett.*, 2004, **4**, 253–256.
29. Star, A., Steuerman, D. W., Heath, J. R., Stoddart, J. F. *Angew. Chem. Int. Ed.*, 2002, **41**, 2508–2512.
30. Zheng, M., Jagota, A., Strano, M. S., Santos, A. P., Barone, P., Chou, S. G., Diner, B. A., Dresselhaus, M. S., McLean, R. S., Onoa, G. B., Samsonidze, G. G., Semke, E. D., Usrey, M., Walls, D. J. *Science*, 2003, **302**, 1545–1548.
31. Zheng, M., Jagota, A., Semke, E. D., Diner, B. A., McLean, R. S., Lustig, S. R., Richardson, R. E., Tassi, N. G. *Nat. Mater.*, 2003, **2**, 338–342.
32. Heller, D. A., Jeng, E. S., Yeung, T.-K., Martinez, B. M., Moll, A. E., Gastala, J. B., Strano, M. S. *Science*, 2006, **311**, 508–11.
33. Tu, X., Manohar, S., Jagota, A., Zheng, M. *Nature*, 2009, **460**, 250–253.
34. McHale, R., Patterson, J. P., Zetterlund, P. B., O'Reilly, R. K. *Nat. Chem.*, 2012, **4**, 491–497.
35. Kang, Y., Pitto-Barry, A., Maitland, A., O'Reilly, R. K. *Polym. Chem.*, 2015, **6**, 4984–4992.
36. McHale, R., OReilly, R. K. *Macromolecules*, 2012, **45**, 7665–7675.
37. Badi, N., Lutz, J.-F. *Chem. Soc. Rev.*, 2009, **38**, 3383–3390.
38. Zhang, K., Fahs, G. B., Aiba, M., Moore, R. B., Long, T. E. *Chem. Commun.*, 2014, **50**, 9145–9148.
39. Hua, Z., Pitto-Barry, A., Kang, Y., Kirby, N., Wilks, T. R., O'Reilly, R. K. *Polym. Chem.*, 2016, **268**, 1728–1731.
40. Imin, P., Imit, M., Adronov, A. *Macromolecules*, 2012, **45**, 5045–5050.
41. Strano, M. S., Dyke, C. A., Usrey, M. L., Barone, P. W., Allen, M. J., Shan, H., Kittrell, C., Hauge, R. H., Tour, J. M., Smalley, R. E. *Science*, 2003, **301**, 1519–1522.
42. Overbeek, J. T. G. *J. Colloid Interface Sci.*, 1977, **58**, 408–422.

43. Dresselhaus, M. S., Jorio, A., Hofmann, M., Dresselhaus, G., Saito, R. *Nano Lett.*, 2010, **10**, 751–758.

44. Dresselhaus, M. S., Dresselhaus, G., Saito, R., Jorio, A. *Phys. Rep.*, 2005, **409**, 47–99.

45. Doorn, S. K. *J. Nanosci. Nanotechnol.*, 2005, **5**, 1023–1034.

46. Strano, M. S., Zheng, M., Jagota, A., Onoa, G. B., Heller, D. A., Barone, P. W., Usrey, M. L. *Nano Lett.*, 2004, **4**, 543–550.

47. Doorn, S. K., Heller, D. A., Barone, P. W., Usrey, M. L., Strano, M. S. *Appl. Phys. A*, 2004, **78**, 1147–1155.

48. Strano, M. S., Doorn, S. K., Haroz, E. H., Kittrell, C., Hauge, R. H., Smalley, R. E. *Nano Lett.*, 2003, **3**, 1091–1096.

49. Heller, D. A., Barone, P. W., Swanson, J. P., Mayrhofer, R. M., Strano, M. S. *J. Phys. Chem. B*, 2004, **108**, 6905–6909.

50. Brown, S., Jorio, A., Corio, P., Dresselhaus, M., Dresselhaus, G., Saito, R., Kneipp, K. *Phys. Rev. B*, 2001, **63**, 1–8.

51. Weisman, R. B., Bachilo, S. M. *Nano Lett.*, 2003, **3**, 1235–1238.

52. Rice, N. A., Subrahmanyam, A. V., Laengert, S. E., Adronov, A. *J. Polym. Sci. Pol. Chem.*, 2015, **53**, 2510–2516.

TOC Graphic